Available online at www.sciencedirect.com
ScienceDirect
Journal of Hazardous Materials 158 (2008) 287–292
Journal of Hazardous Materials
www.elsevier.com/locate/jhazmat

# Characterization and photocatalytic properties of Ni-doped $Sr_{10}Bi_6O_{24-y}$

Gaoke Zhang *, Jin Zhou, Xinmiao Ding, Yanjun Hu, Junwei Xie

*School of Resources and Environmental Engineering, Wuhan University of Technology, Luoshi Road 122, Wuhan 430070, PR China*

Received 4 August 2007; received in revised form 30 October 2007; accepted 18 January 2008
Available online 12 February 2008

**Abstract**

The compound $Sr_{10}Bi_6O_{24-y}$ doped with Ni was prepared by solid-state reaction method. The obtained powders were characterized by X-ray diffraction (XRD), scanning electron microscopy (SEM), UV–vis diffuse reflectance spectra and X-ray photoemission spectra (XPS). The Ni-doped $Sr_{10}Bi_6O_{24-y}$ samples assume a cubic perovskite structure with space group Fm3m (2 2 5). Bi in $Sr_{10}Bi_6O_{24-y}$ exists in the valence state of Bi(II). Photocatalytic activities of the prepared samples were evaluated using acid red G as a model organic compound. The results show that doping with 0.5 wt.% Ni can significantly improve the photoactivity of the compound $Sr_{10}Bi_6O_{24-y}$.


*Keywords:* Photocatalytic; Acid red G; Bismuth; Strontium; Ni-doped; Perovskite

## 1. Introduction

Photocatalytic methods, using semiconductors, such as $TiO_2$, have attracted extensive attention, because they provide a promising strategy for cleaning polluted air or water [1]. Previous studies have shown that such semiconductors can degrade most kinds of persistent organic pollutant, such as dyes, pesticide, detergents and volatile organic compounds, under UV-light irradiation [1–4]. However, the fast recombination rate of photogenerated electron/hole pairs hider the commercialization of this technology [1,2]. As a result, a number of photocatalysts have been investigated with the aim of improving catalyst activity and stability in the irradiated aqueous environment.

In oxide semiconductors, the conduction band levels of small-band-gap semiconductors are usually low because the deep valence bands are formed by O2p, which is a major problem for developing stable oxide photocatalysts. To find a breakthrough, it is indispensable to control the valence band with orbital of some elements instead of O2p [5]. Accordingly, a valence band or an electron donor level consisting of orbitals of some elements, except for O2p; has to be formed to make the band gaps or the energy gaps narrow [6].

It has been found that bismuth is a potential candidate for such a valence band control element. Recently, many attentions have been paid for developing photocatalysts containing bismuth with high activities for environmental applications and/or water splitting, such as $BiWO_4$ [5], $BiVO_4$ [7–9], $CaBi_2O_4$ [10], $Bi_2Ti_2O_7$ [11] and $Bi_4Ti_3O_{12}$ [12].

$Sr_{10}Bi_6O_{24-y}$ was first reported by Bokhimi and Portilla [13]. But its photocatalytic property has never been investigated. In this paper, the compound Ni-doped $Sr_{10}Bi_6O_{24-y}$ was synthesized by a simple solid-state reaction method and its photocatalytic property was first studied for the degradation of acid red G.

## 2. Experiment

The $Sr_{10}Bi_6O_{24-y}$ powder was synthesized by a solid-state reaction method. $Bi_2O_3$ and $Sr(NO_3)_2$ with the purity of 99.95% were used as raw materials. Mixed raw materials with the stoichiometric proportion were ground with an agate mortar for 30 min, sintered in a crucible at 900 °C for 2 h, and then cooled to room temperature. The obtained samples were also manually grinded with an agate mortar again.

* Corresponding author.
*E-mail address:* gkzhang@whut.edu.cn (G. Zhang).

0304-3894/$ – see front matter © 2008 Elsevier B.V. All rights reserved.
doi:10.1016/j.jhazmat.2008.01.110

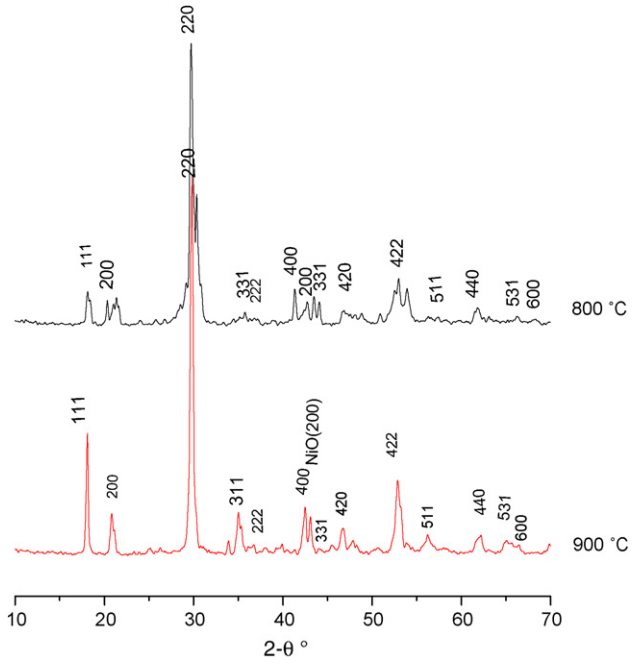


Fig. 1. X-ray powder diffraction patterns of photocatalysts calcined at different temperature.

The samples of Ni-doped $Sr_{10}Bi_6O_{24-y}$ were also prepared by solid-state reaction, the ground mixtures of $Bi_2O_3$, $Sr(NO_3)_2$ and $Ni(NO_3)_2{\cdot}6H_2O$ were sintered at the same condition.

Photocatalytic properties of as-prepared samples were evaluated using acid red G as a model organic compound. The decolorization of acid red G solution was carried out in a 500 ml Pyrex glass vessel with constant magnetic stirring. A 20 W UV lamp with a maximum emission at about 254 nm was used as the light source. Reaction suspension was prepared by adding the prepared samples (2 g/L) into 150 mL aqueous acid red G solution (50 mg/L). The absorption/degradation equilibrium of the suspensions was established after magnetically stirring in a dark condition for 10 min. No significant change in the concentration of acid red G in the suspensions was found after magnetically stirring for 2 h without UV irradiation.

## 3. Results and discussions

### 3.1. Characterization of the prepared powders

#### 3.1.1. X-ray powder diffraction

X-ray powder diffraction pattern were carried out on a Rigaku D/MAX-RB powder X-ray diffractometer with Cu Kα radiation operating at 40 kV and 50 mA, and employing a scanning rate of 0.02° and speed of 3° $min^{-1}$, in the range of 2$\theta$ from 10° to 70°.

Fig. 1 shows the effects of calcining temperature on the crystallization of 0.5 wt.% Ni-doped $Sr_{10}Bi_6O_{24-y}$. The results of X-ray diffraction (XRD) patterns confirmed that the Ni-doped $Sr_{10}Bi_6O_{24-y}$ samples assume a cubic perovskite structure with space group Fm3m (2 2 5) [13] as those given in JCPDS data cards (JCPDS 81-2408), which had been well crystallized when

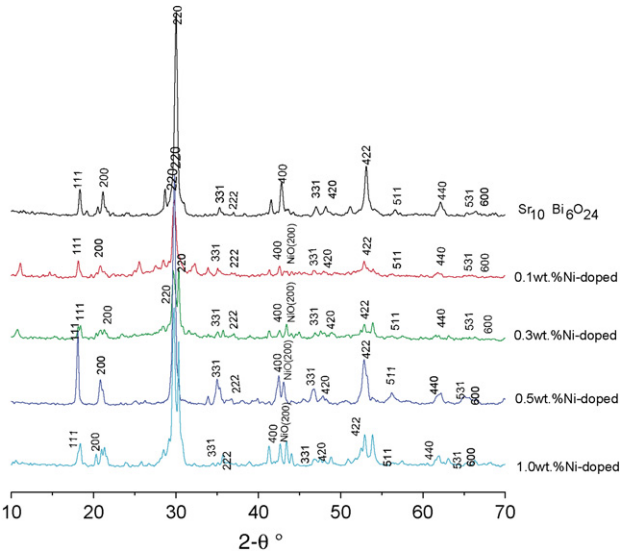


Fig. 2. X-ray powder diffraction patterns of photocatalysts with different metal doping concentration.

calcined at 800 °C for 2 h. The strongest peak (2 0 0) of oxide nickel species was observed at Ni-doped $Sr_{10}Bi_6O_{24-y}$ sample and the other peaks in the XRD patterns can be readily identified and indexed using the standard XRD data for the $Sr_{10}Bi_6O_{24-y}$. With further increasing the annealing temperature up to 900 °C, XRD patterns of the prepared samples do not show any significant variation and the peaks in it became sharper and the full width at half maximum decreased, which indicates a better crystallinity and an increase in grain size when sintering at higher temperature.

The effects of Ni doping on the crystallization of $Sr_{10}Bi_6O_{24-y}$ were also examined, as shown in Fig. 2, the doping concentration of Ni has no great influence on the structure and crystallization of $Sr_{10}Bi_6O_{24-y}$. All the prepared samples sintered at 900 °C for 2 h had been well crystallized. The XRD patterns do not show any significant variation and the strongest peak (2 0 0) of oxide nickel species became sharper with increasing Ni doping concentration, which indicates that the Ni-doped $Sr_{10}Bi_6O_{24-y}$ maintains a cubic structure similar to the $Sr_{10}Bi_6O_{24-y}$ even under extensive modification by Ni and the nickel in the catalyst exists in the state of NiO.

#### 3.1.2. Scanning electron microscope (SEM)

Scanning electron microscopy was performed on JSM-5610LV scanning electron microscope.

From the SEM images shown in Fig. 3, it can be found that the well-crystallized composite systems of $Sr_{10}Bi_6O_{24-y}$, 0.5 wt.% Ni-doped $Sr_{10}Bi_6O_{24-y}$ and 1.0 wt.% Ni-doped $Sr_{10}Bi_6O_{24-y}$ exhibit similar morphologies. The micrographs depict they are made up of polyhedron crystal grains without distinct facet and sharp angle. The microstructure of 0.5 wt.% Ni-doped $Sr_{10}Bi_6O_{24-y}$ (Fig. 3b) and 1.0 wt.% Ni-doped $Sr_{10}Bi_6O_{24-y}$ samples (Fig. 3c) show little change compared with that of the pure $Sr_{10}Bi_6O_{24-y}$ (Fig. 3a). Some small grains congregated on the corners are embedding into big grains. It may be the oxide nickel species, which is coincide with the XRD results.

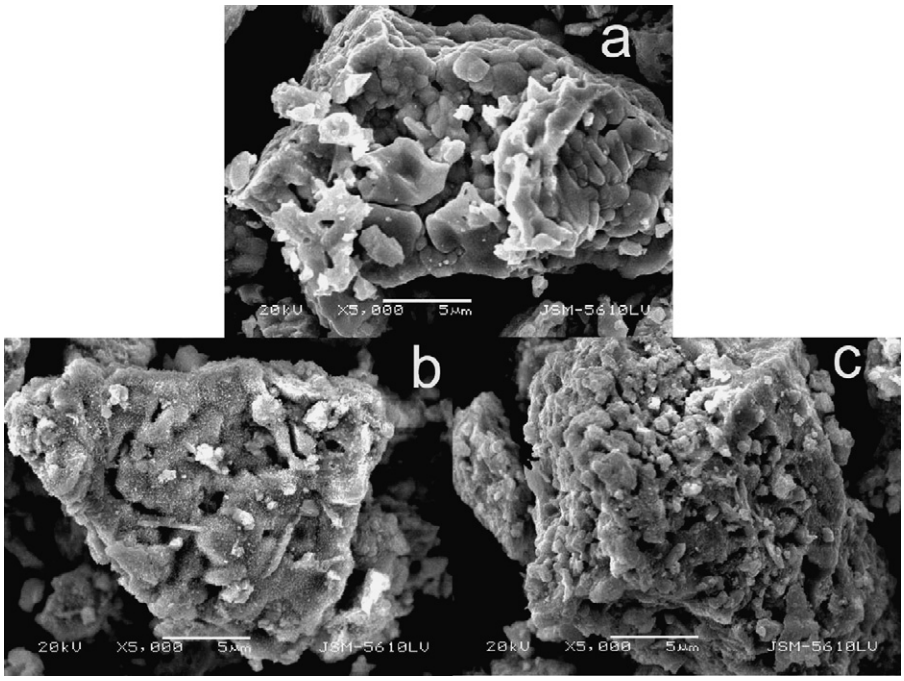


Fig. 3. SEM images (a) $Sr_{10}Bi_6O_{24-y}$, (b) 0.5 wt.% Ni-doped $Sr_{10}Bi_6O_{24-y}$ and (c) 1.0 wt.% Ni-doped $Sr_{10}Bi_6O_{24-y}$.

### 3.1.3. Diffuse reflectance spectra

Diffuse reflectance spectral analysis of the photocatalyst was determined by UV–vis spectrometer (UV-2100).

It is well known that light absorption by the material and the migration of the light-induced electrons and holes are the most key factors controlling a photocatalytic reaction, which is relevant to the electronic structure characteristics of the materials [10,14]. Fig. 4 shows DR spectra for the as-prepared samples. The band gap absorption edge of the catalysts $Sr_{10}Bi_6O_{24-y}$ and Ni-doped $Sr_{10}Bi_6O_{24-y}$ obtained is determined to be 724 nm and 693 nm, corresponding to the band gap energy of 1.71 eV and 1.78 eV, respectively.

### 3.1.4. X-ray photoelectron spectroscopy (XPS)

The valence state of Bi was analyzed by X-ray photoelectron spectroscopy, using a VG Scientific ESCALAB Mark II spectrometer equipped with two ultrahigh-vacuum (UHV) chambers; the pressure in the chambers during the experiments was about $10^{-7}$ Pa. A Mg Kα X-ray source was used. The analyzer was operated at 20 eV pass energy for high-resolution spectra (Fig. 5).

The XPS binding energy is mostly determined by the oxidation state of the studied atom but is also very sensitive to its chemical environment. Bi4f5/2 and Bi4f7/2 in $Bi_2O_3$ have been reported as 164.1–164.9 eV and 158.5–159.5 eV, respectively. And the binding energy (B.E.) values in BiO have been reported as 157.2 eV and 162.3 eV [15–17]. In the Bi4f B.E. region, the B.E. values associates with the main peaks 4f7/2 (157.3 eV) and

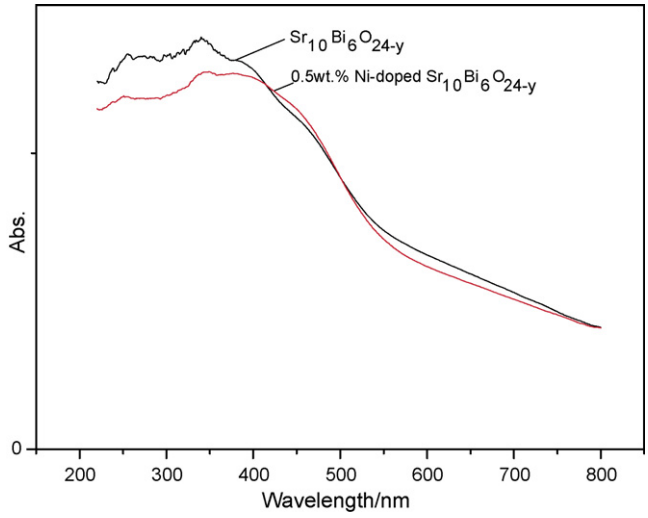


Fig. 4. UV–vis diffuse reflectance spectra.

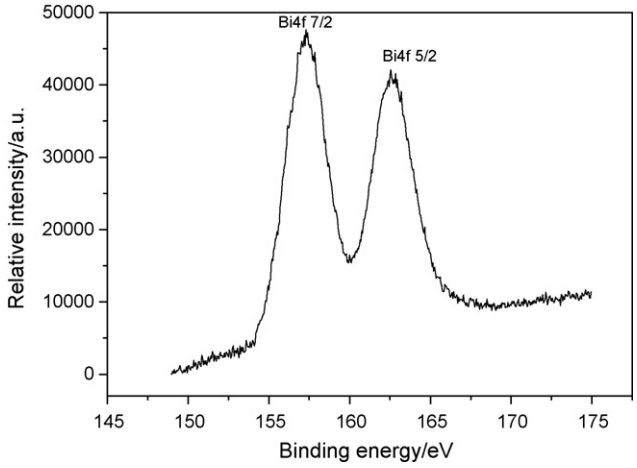


Fig. 5. High-resolution XPS spectra of Bi4f.

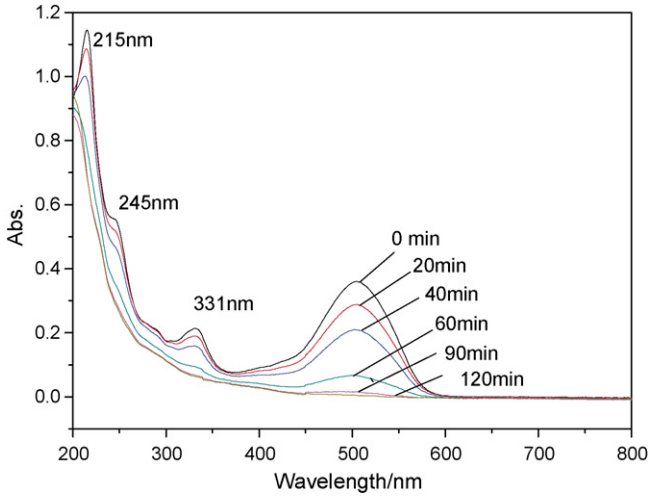


Fig. 6. UV–vis absorption spectra profile changes of photocatalytic degradation of 50 mg/L acid red G by Ni-doped $Sr_{10}Bi_6O_{24-y}$ at different times: (1) 0 min; (2) 20 min; (3) 40 min; (4) 60 min; (5) 90 min; (6) 120 min.

4f5/2 (162.5 eV) are in good agreement with the data for BiO powders. Although the present XPS analyses cannot provide definite information due to the inherent limitation in the method and/or the unavailability of appropriate reference compounds, it is highly probable that Bi in $Sr_{10}Bi_6O_{24-y}$ exists in the valence state as in BiO, which may be attributed to the oxygen vacancy [13].

### 3.2. Photocatalytic activity of the prepared samples

#### 3.2.1. UV–vis absorption spectra

The changes in the UV–vis absorption spectra of acid red G during the photocatalytic degradation by the sample prepared at 900 °C at different irradiation times, which were recorded by UV–vis spectrometer (UV-160), were given in Fig. 6. The result shows four distinctive peaks at 215 nm, 245 nm, 331 nm and 505 nm. The peak at 505 nm, which is with respect to the nitrogen to nitrogen double bond (–N=N–), was used to monitor

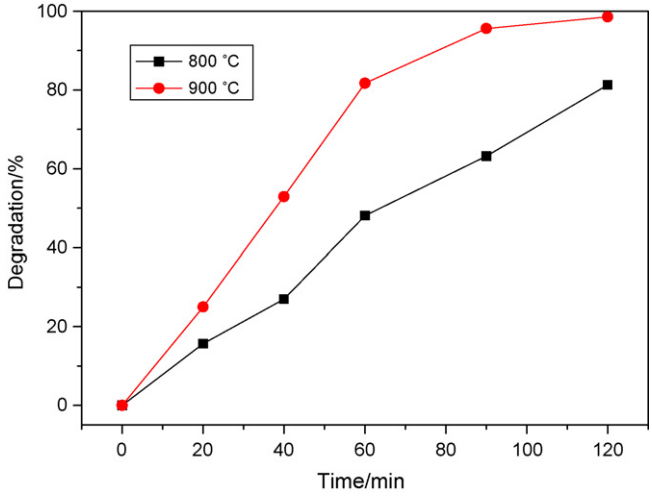


Fig. 7. Photocatalytic properties of Ni-doped $Sr_{10}Bi_6O_{24-y}$ obtained at different temperature.

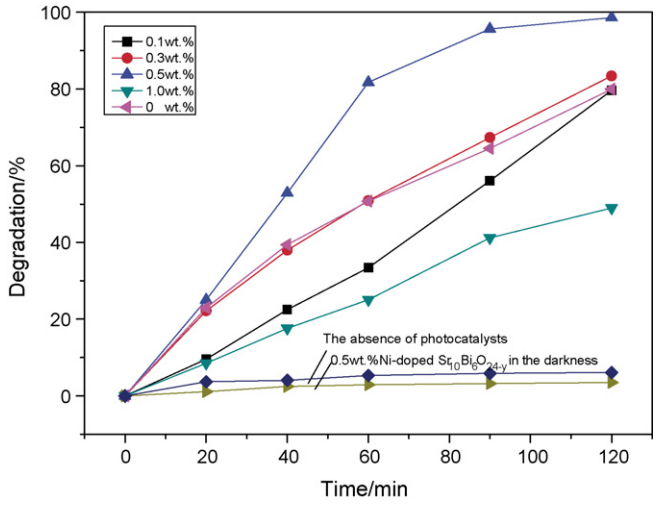


Fig. 8. Effects of Ni doping on the photocatalytic activity of $Sr_{10}Bi_6O_{24-y}$.

the effect of the degradation of acid red G by the catalyst. Its intensity rapidly decreases with increasing the photocatalytic reaction time, which indicates a rapid degradation of azo dye. The decrease of the peaks at 215 nm, 245 nm and 331 nm, which are with respect to aromatic rings [18], means the destruction of the molecular structure of acid red G with increase in the photocatalytic reaction time. The color of the suspension became light gradually and disappeared ultimately.

#### 3.2.2. Effect of calcined temperature

The effect of calcined temperature on the photocatalytic activity of Ni-doped $Sr_{10}Bi_6O_{24-y}$ was examined. As shown in Fig. 7, it can be seen that the degradation rate of acid red G increased with the increasing annealing temperature from 800 °C to 900 °C, which may be attributed to the better crystallinity.

#### 3.2.3. Effect of the Ni doping

Fig. 8 shows the effect of the Ni doping on the photocatalytic activity of $Sr_{10}Bi_6O_{24-y}$. From the results, the doping concentration of Ni in the prepared samples has a great effect

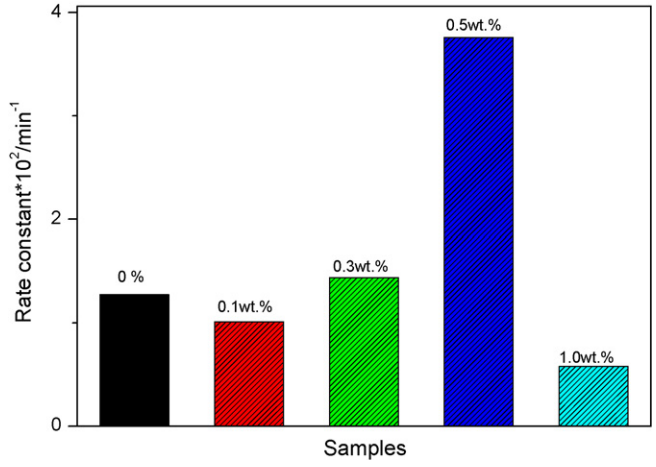


Fig. 9. The photocatalytic reaction rate constants of the obtained samples.

upon their activities decolorize acid red G solution. The photocatalytic activity of Ni-doped $Sr_{10}Bi_6O_{24-y}$ increases with the increasing Ni doping. The 0.5 wt.% Ni-doped sample shows the highest activity, which is much higher than that of un-doped sample. The photocatalytic activity of the Ni-doped sample markedly decreased with the increasing Ni doping to 1.0 wt.%. This suggests that the optimum Ni doping amount exists. The acid red G was hardly degraded by Ni-doped $Sr_{10}Bi_6O_{24-y}$ in the darkness or UV irradiation in the absence of photocatalysts. It suggests that both UV irradiation and photocatalysts are necessary for the effective destruction of acid red G by the catalysts.

### 3.2.4. Kinetics of photcatalytic degradation of acid red G

Most of the heterogeneous photocatalytic degradation reaction follow Langmuir–Hinshelwood model [19]. When the initial concentration of acid red G is low, the relation between C and the reaction time $t$ can be described by the following equation [20–22]:

$$\ln\left(\frac{C_0}{C_t}\right) = k\,(\mathrm{min}^{-1})t + a \quad (1)$$

where $k$ is the apparent reaction rate constant, $C_0$ the initial concentration of aqueous acid red G and $C_t$ is the concentration of aqueous acid red G at the reaction time of $t$. From the results in Fig. 9, $Sr_{10}Bi_6O_{24-y}$ doped with 0.5 wt.% Ni ions has the highest rate constant and the $k$ value reaches $3.76 \times 10^{-2}\ \mathrm{min}^{-1}$, which is much higher than $1.27 \times 10^{-2}\ \mathrm{min}^{-1}$ of un-doped sample.

It was widely accepted that the photoactivities of doped catalysts are related to the dopant trap site. The trapped charges in photocatalytic reaction should be transferred to the interface to initiate the photoreactions [23]. Metal ion dopants influence the photoreactivity of catalysts by acting as electron (or hole) traps and by altering the $e^-/h^+$ pair recombination rate [24–26]. That is, the doped metallic ions may transfer the electrons and make a good separation effect, and may be the recombination center of electron–hole pairs which is in contrast with separation. The role of metallic ions is in connection with their distribution in the catalyst that was determined by doping mode and concentration. As reported by Zou et al. [27], nickel was shown to facilitate the excited electron transfer and hence suppress efficiently the recombination of photoproduced electron–hole. Gurunathan [28] found that the photocatalytic activity on Ni-doped γ-$Bi_2O_3$ was much higher than non-doped γ-$Bi_2O_3$. Here, the photocatalytic activity of $Sr_{10}Bi_6O_{24-y}$ is improved efficiently since the Ni acts as electron traps and thus facilitates the charge separation. At low concentration, NiO serves as an electron ($e^-$) trapper and prohibits the recombination of holes and electrons.

The observed photoactivity decrease in the prepared samples with increasing of the Ni doping concentration is probably due to the large doping amount of Ni which can lead to the dopants are more likely to serve as recombination centers than as trap sites for eventual charge transfer at the interface. Such phenomena were also reported by other researchers [29–31].

## 4. Conclusions

Ni-doped $Sr_{10}Bi_6O_{24-y}$ compound was synthesized by solid-state reaction method. Ni doping does not change the crystal structure of the compound $Sr_{10}Bi_6O_{24-y}$ and the Ni-doped $Sr_{10}Bi_6O_{24-y}$ samples assume a cubic perovskite structure with space group Fm3m (2 2 5). Bi in $Sr_{10}Bi_6O_{24-y}$ exists in the valence state of Bi(II). The experimental results show that the low concentration of Ni-doping can significantly increase the photocatalytic activity of $Sr_{10}Bi_6O_{24-y}$ crystals. There is an optimum amount of Ni doping, which leads to a maximum of the photocatalytic activity. The 0.5 wt.% Ni-doped sample shows the highest activity, which was much higher than that of un-doped sample.

## Acknowledgements

This work was supported by NCET05-0662, National Basic Research Program of China (973 Program) 2007CB613302 and Wuhan University of Technology.

## References

[1] M.R. Hoffmann, S.T. Martin, W. Choi, D.W. Bahnemann, Applications of semiconductor photocatalysis, Chem. Rev. 95 (1995) 69–96.
[2] C. Wang, J. Zhao, X. Wang, B. Mai, G. Sheng, P. Peng, J. Fu, Preparation, characterization and photocatalytic activity of nano-sized ZnO/$SnO_2$ coupled photocatalysts, Appl. Catal. B: Environ. 39 (2002) 269–279.
[3] A.L. Linsebigler, G.Q. Lu, J.T. Yates, Environmental applications of semiconductor photocatalysis, Chem. Rev. 95 (1995) 735–758.
[4] T. Torimoto, S. Ito, S. Kuwabata, H. Yoneyama, Effects of absorbents used as supports for titanium dioxide loading on photocatalytic degradation of propyzamide, J. Environ. Sci. Technol. 30 (1996) 1275–1281.
[5] H.B. Fu, C.S. Pan, W.Q. Yao, Y.F. Zhu, Visible-light-induced degradation of rhodamine B by nanosized $Bi_2WO_6$, J. Phys. Chem. B 109 (2005) 22432–22439.
[6] A. Kudo, Photocatalyst materials for water splitting, Catal. Surv. Asia 7 (2003) 31–38.
[7] S. Tokunaga, H. Kato, A. Kudo, Selective preparation of monoclinic and tetragonal $BiVO_4$ with scheelite structure and their photocatalytic properties, Chem. Mater. 13 (2001) 4624–4628.
[8] S. Kohtani, J. Hiro, N. Yamamoto, A. Kudo, K. Tokumura, R. Nakagaki, Adsorptive and photocatalytic properties of Ag-loaded $BiVO_4$ on the degradation of 4-n-alkylphenols under visible light irradiation, Catal. Commun. 6 (2005) 185–189.
[9] A. Kudo, K. Ueda, H. Kato, I. Mikami, Photocatalytic $O_2$ evolution under visible light irradiation on $BiVO_4$ in aqueous $AgNO_3$ solution, Catal. Lett. 53 (1998) 229–230.
[10] J. Tang, Z. Zou, J. Ye, Efficient photocatalytic decomposition of organic contaminants over $CaBi_2O_4$ under visible light irradiation, Angew. Chem. Int. Ed. 43 (2004) 4463–4466.
[11] W.F. Yao, H. Wang, X.H. Xu, J.T. Zhou, X.N. Yang, Y. Zhang, S.X. Shang, Photocatalytic property of bismuth titanate $Bi_2Ti_2O_7$, Appl. Catal. A. Gen. 259 (2004) 29–33.
[12] W.F. Yao, X.H. Xu, H. Wang, J.T. Zhou, X.N. Yang, Y. Zhang, S.X. Shang, B.B. Huang, Photocatalytic property of perovskite bismuth titanate, Appl. Catal. B: Envrion. 52 (2004) 109–116.
[13] Bokhimi, M. Portilla, Oxygen and the formation of new ordered perovskite-based structures in the Bi–Sr–O system, J. Solid State Chem. 105 (1993) 371–377.

[14] J. Tang, Z. Zou, J. Ye, Effect of substituting Sr and Ba for Ca on the structure properties and photocatalytic behaviors of $CaIn_2O_4$, Chem. Mater. 16 (2004) 1644–1649.
[15] W.E. Morgan, W.J. Stec, J.R. Van Wazer, Inner-orbital binding-energy shifts of antimony and bismuth compounds, Inorg. Chem. 12 (1973) 953–955.
[16] T.R. Felthouse, P.B. Fraundorf, R.M. Friedman, C.L. Schosser, Expanded lattice ruthenium pyrochlore oxide catalysts. I. Liquid-phase oxidations of vicinal diols, primary alcohols, and related substrates with molecular oxygen, J. Catal. 127 (1991) 393–420.
[17] A. Gulino, S. La Delfa, I. Fragala', R.G. Egdell, Low-temperature stabilization of tetragonal zirconia by bismuth, Chem. Mater. 8 (1996) 1287–1291.
[18] P. Qu, J. Zhao, T. Shen, H. Hidaka, $TiO_2$-assisted photodegradation of dyes: a study of two competitive primary processes in the degradation of RB in an aqueous $TiO_2$ colloidal solution, J. Mol. Catal. A: Chem. 129 (1998) 257–268.
[19] D.F. Ollis, E. Pelizzetti, N. Serpone, Contaminant degradation in water, Environ. Sci. Technol. 19 (1985) 480–484.
[20] H. AI-Ekabi, N. Serpone, Kinetic studies in heterogeneous photocatalysis. 1. Photocatalytic degradatlon of chlorinated phenols in aerated aqueous solutions over TIO, supported on a glass matrix, J. Phys. Chem. 92 (1988) 5726–5731.
[21] A. Valentine Rupa, D. Manikandan, D. Divakar, T. Sivakumar, Effect of deposition of Ag on $TiO_2$ nanoparticles on the photodegradation of reactive yellow-17, J. Hazard. Mater. 147 (2007) 906–913.
[22] G. Zhang, J. Gong, X. Zou, F. He, H. zhang, Q. Zhang, Y. Liu, X. Yang, B. Hu, Photocatalytic degradation of azo dye acid red G by $KNb_3O_8$ and the role of potassium in the photocatalysis, Chem. Eng. J. 123 (2006) 159–164.
[23] W.F. Yao, H. Wang, S.X. Shang, X.H. Xu, X.N. Yang, Y. Zhang, M. Wang, Photocatalytic property of Zn-modified bismuth titanate, J. Mol. Catal. A: Chem. 198 (2003) 343–348.
[24] W. Choi, A. Termin, M.R. Hoffman, The role of metal ion dopants in quantum-sized $TiO_2$: correlation between photoreactivity and charge carrier recombination dynamics, J. Phys. Chem. 98 (1994) 13669–13679.
[25] M. Gratzel, R.F. Howe, Electron paramagnetic resonance studies of doped $TiO_2$ colloids, J. Phys. Chem. 94 (1990) 2566–2572.
[26] Mu Wei, J.M. Herrmann, P. Pichat, Room temperature photocatalytic oxidation of liquid cyclohexane into cyclohexanone over pure and modified titanium(IV) oxide, Catal. Lett. 3 (1989) 73–84.
[27] Z.G. Zou, J.H. Ye, K. Sayama, H. Arakawa, Direct splitting of water under visible light irradiation with an oxide semiconductor photocatalyst, Nature 414 (2001) 625–627.
[28] K. Gurunathan, Photocatalytic hydrogen production using transition metal ions-doped $\gamma$-$Bi_2O_3$ semiconductor particles, Int. J. Hydrogen Energy 29 (2004) 933–940.
[29] W.F. Yao, H. Wang, X.H. Xu, Y. Zhang, X.N. Yang, S.X. Shang, Y.H. Liu, J.T. Zhou, Characterization and photocatalytic properties of Ba doped $Bi_{12}TiO_{20}$, J. Mol. Catal. A: Chem. 202 (2003) 305–311.
[30] H. Yu, X.J. Li, S.J. Zheng, W. Xu, Photocatalytic activity of $TiO_2$ thin film non-uniformly doped by Ni, Mater. Chem. Phys. 97 (2006) 59–63.
[31] T. Sreethawong, Y. Suzuki, S. Yoshikawa, Photocatalytic evolution of hydrogen over mesoporous $TiO_2$ supported NiO photocatalyst prepared by single-step sol–gel process with surfactant template, Int. J. Hydrogen Energy 30 (2005) 1053–1062.